

Ordering near the percolation threshold in models of 2D interacting bosons with quenched dilution

N. Bray-Ali,¹ J. E. Moore,^{1,2} T. Senthil,³ and A. Vishwanath^{1,2}

¹*Department of Physics, University of California, Berkeley, CA 94720*

²*Materials Sciences Division, Lawrence Berkeley National Laboratory, Berkeley, CA 94720*

³*Department of Physics, Massachusetts Institute of Technology, Cambridge MA 02139*

(Dated: July 25, 2005)

Randomly diluted quantum boson and spin models in two dimensions combine the physics of classical percolation with the well-known dimensionality dependence of ordering in quantum lattice models. This combination is rather subtle for models that order in two dimensions but have no true order in one dimension, as the percolation cluster near threshold is a fractal of dimension between 1 and 2: two experimentally relevant examples are the $O(2)$ quantum rotor and the Heisenberg antiferromagnet. We study two analytic descriptions of the $O(2)$ quantum rotor near the percolation threshold. First a spin-wave expansion is shown to predict long-ranged order, but there are statistically rare points on the cluster that violate the standard assumptions of spin-wave theory. A real-space renormalization group (RSRG) approach is then used to understand how these rare points modify ordering of the $O(2)$ rotor. A new class of fixed points of the RSRG equations for disordered 1D bosons is identified and shown to support the existence of long-range order on the percolation backbone in two dimensions. These results are relevant to experiments on bosons in optical lattices and superconducting arrays, and also (qualitatively) for the diluted Heisenberg antiferromagnet $\text{La}_2(\text{Zn,Mg})_x\text{Cu}_{1-x}\text{O}_4$.

PACS numbers: 05.30.Jp, 64.60.Ak, 74.81.-g, 75.10.Jm, 75.10.Nr, 75.40.Cx, 75.40.Mg

I. INTRODUCTION

The physics of classical lattice percolation has been used to model a great variety of physical systems with considerable success,¹ and recent results on 2D percolation have put this classical theory on a firm mathematical footing.² Several materials of current interest are well described by combining random dilution with lattice quantum degrees of freedom, as in a magnetic material in which some quantum spins have been removed by chemical dilution.³ Aside from its interest as a microscopic description of dilution in materials, percolation is important as the simplest nondeterministic process for generating a “fractal”, an object of fractional dimensionality:⁴ as explained later in this introduction, there is a geometric phase transition in randomly diluted lattice systems with a fractal structure at the transition point.

The focus of this paper is on models for randomly diluted interacting bosons. These models describe superconducting Josephson-junction arrays with only onsite interactions and a finite density of defective junctions, or bosons in optical lattices where some sites remain empty. Percolation of superconductivity at short length scales has also been discussed as a model for inhomogeneity observed by scanning tunneling microscopy on the high-temperature superconductor BSCCO.⁵ Finally, the $O(2)$ rotor is qualitatively similar to the nearest-neighbor $s = 1/2$ antiferromagnetic Heisenberg model in that both have long-range order in two dimensions but only algebraic correlations in one dimension. The diluted Heisenberg model has been studied numerically^{3,6,7} and in neutron scattering experiments on $\text{La}_2(\text{Zn,Mg})_x\text{Cu}_{1-x}\text{O}_4$.³

Our interest in interacting bosons suggests that we con-

sider the diluted $O(2)$ quantum rotor model. More generally, the $O(N)$ quantum rotor model⁸ has an N component unit vector \hat{n}_i living at every lattice site i . The effect of dilution is incorporated by defining the symbol α_{ij} to be unity if the bond ij is present in the diluted system, and zero otherwise. For concreteness, we consider bond dilution though the results are more general. Then, the Hamiltonian for a particular realization of the dilution $\{\alpha_{ij}\}$ is given by:

$$H = \frac{U}{2} \sum_i \mathbf{L}_i^2 - J \sum_{\langle ij \rangle} \alpha_{ij} \hat{n}_i \cdot \hat{n}_j \quad (1)$$

where, U and J are positive coupling constants, and the components of the angular momenta $[\mathbf{L}]_{\alpha\beta}$ are given by $[\mathbf{L}]_{\alpha\beta} = p_\alpha n_\beta - p_\beta n_\alpha$ ($\alpha \neq \beta$) where $[n_\alpha, p_\beta] = i\delta_{\alpha\beta}$, and the greek indices take values from 1 to N . Thus the kinetic energy part of the Hamiltonian is just $\mathbf{L}^2 = \sum_{\alpha < \beta} L_{\alpha\beta}^2$. For undiluted lattices of dimension $d \geq 2$, the quantum $O(N)$ rotor model has long-range order, as long as quantum fluctuations (measured by the ratio U/J) are below some non-zero, N -dependent, critical value $(U/J)_c$. However, a chain of quantum rotors has no long-range order for any $N \geq 2$ unless $U = 0$.⁸

In a certain sense, a planar material with a large fraction of diluted bonds (or sites) has geometry between one- and two-dimensions. When the dilution fraction p reaches a lattice-dependent critical value ($p_c = 1/2$ for square lattice bond dilution), there is a geometric phase transition: for $p < p_c$ there is an infinite nearest-neighbor connected cluster of undiluted sites for essentially all realizations of dilution, while for $p > p_c$ there is no infinite cluster.¹ At threshold ($p = p_c$), the number of bonds of

the cluster, $N(r)$, contained in a small circle of radius r around a given bond of the cluster: $N(r) \sim r^{d_f}$, with the “fractal” dimension $d_f = 91/48 \approx 1.896$ [Ref. 1]. Now, an undiluted chain of sites has $N(r) \sim r$ and an undiluted square lattice, $N(r) \sim r^2$, so, in this sense, the cluster is “between” one- and two-dimensions. Note, however, that other geometric properties of the cluster have other dimensionalities, some, in fact, less than one.¹

Allowing quantum fluctuations ($U \neq 0$), raises an important question about the nature of order in diluted, planar systems: Does the order on the critical cluster which exists for $U = 0$ persist for non-zero U ? Early numerical and analytic work on the diluted Heisenberg model suggested that long-range order vanishes before the percolation threshold,^{9,10} although recent numerics disagree.^{6,11} This paper begins to resolve this question analytically by coupling a spin-wave approach to a complementary real-space renormalization group (RSRG) analysis.

The spin-wave approximation, described in Section II, provides a natural first step for describing the effects of weak quantum fluctuations on the $O(N)$ rotor model at threshold. We show that the *fracton* dimension d_s of the cluster, which is close to $4/3$ for percolation in any dimension,¹ is the relevant dimension to consider when discussing ordering near percolation threshold. Since the fracton dimension is greater than one, quantum fluctuations of the order parameter on an *average* site of the cluster are small, according to our computation. We also cite a rigorous result that implies, within the framework of the spin-wave approximation, that all sites have small quantum fluctuations provided that $p < p_c$.

In principle, this is not enough to argue that the superfluid order is stable to quantum fluctuations. One might worry whether the stability to quantum fluctuations persists beyond the weak quantum fluctuations allowed by the spin-wave approximation. Further, at $p = p_c$ where the spin-wave approach only describes the behavior of an *average* site, one might be concerned that quantum fluctuations suppress superfluid order on a set of sites of measure zero on the percolation cluster. If these special sites are such that in their absence the full connectivity of the cluster is lost, then there still may be no true long range order. For instance the order may be destroyed on the long 1D segments connecting the large blobs on the percolation cluster’s backbone (Fig. 1).

In Section III, we identify an effective model for rotors on the cluster backbone that incorporates fluctuations along long links beyond the linear approximation. The physical idea, which we develop in detail is that these fluctuations occur on a qualitatively faster time-scale than fluctuations in the blobs. We refer to this as the slow blob approximation or SBA. Within the SBA, we compute a low-energy effective Hamiltonian for the $O(N)$ rotor model on the percolation cluster. Due to the one-dimensional topology of the backbone, the effective Hamiltonian is a *one*-dimensional $O(N)$ rotor model with strongly-inhomogeneous charging $\{u_i\}$ and exchange $\{j_i\}$

energies:

$$H_{SB} = \sum_i \frac{u_i}{2} \mathbf{L}_i^2 - \sum_i j_i \hat{n}_i \cdot \hat{n}_{i+1}, \quad (2)$$

where the coupling constants $\{j_i\}, \{u_i\}$ are independent, random variables, with distributions $P(j)$ and $R(u)$ respectively. Like the α_{ij} in (1), these coupling constants are randomly distributed. However, the distributions $P(j), R(u)$ are continuous for small $j \ll J$ and small $u \ll U$, respectively. In contrast the α_{ij} have a discontinuous, bimodal distribution. Note that the SBA drastically simplifies the geometry of the problem. In the SBA, the effective model (2) is truly one-dimensional: namely the 1D $O(N)$ rotor model with strong disorder.

To reach this effective description, we focus on the backbone of the incipient infinite cluster. Most bonds lie off the backbone: our physical idea is that these “dangling” bonds will exhibit long-range order if and only if the backbone bonds do so. This is reasonable, since at $U = 0$, the dangling bonds play no role in communicating phase correlations. Moreover, previous work following this line of analysis successfully explains a number of basic phenomena of ordering near percolation threshold. For example, the finite temperature phase diagram in any dimension of *classical* magnets diluted with non-magnetic impurities (e.g. $Rb_p Mn_{1-p} F_2$ which has a large $S = 5/2$ local moment), follows from analyzing backbone thermodynamics.^{1,12,13} Further, for quantum magnets with *discrete* symmetry (such as the transverse field Ising model), backbone physics accounts for the zero temperature phase diagram as well.¹⁴ The present work simply extends the previous treatments to cover *continuous*, *quantum* degrees of freedom.

Recently, the real-space renormalization group approach to quantum systems with strong disorder, perfected by D.S. Fisher in the context of random-exchange Heisenberg antiferromagnetic spin chains,¹⁵ has been extended to the 1D $O(2)$ rotor model with strong disorder by E. Altman et.al.¹⁶ In section IV and V, the machinery of this approach is brought to bear on the effective model in Eq.2. The result indicates that for the $O(2)$ rotor, superfluid order persists at threshold even with a large amount of quantum fluctuation, namely, up to $U/J \approx (U/J)_{KT} \approx \pi^2/4$, where, $(U/J)_{KT}$ is the location of the Kosterlitz-Thouless transition of the clean 1D $O(2)$ rotor model. Section V treats the range $U/J < (U/J)_{KT}$, while section IV discusses the loss of superfluid order which occurs just above $(U/J)_{KT}$.

Section VI concludes the paper with a discussion of the phase diagram of the $O(2)$ rotor model with quenched dilution. Two appendices present details of the real-space renormalization group computations.

II. SPIN WAVES ON THE CRITICAL PERCOLATION CLUSTER

There are two main results of this analysis: First, exactly at threshold ($p = p_c$) and except for certain rare points (“geometric fluctuations”), long-range order is stable to weak quantum fluctuations. Second, away from threshold, on the percolating side ($p < p_c$), long-range order is stable to weak quantum fluctuations on *any* site, for almost all clusters.

Clearly, if $U = 0$ in (1) we are in the classical limit of this model, and the ground state simply has $\hat{n}_i = \text{const.}$ on all sites of a connected cluster. The question that we will address first is, exactly at the percolation threshold, does this long range order on the percolation cluster survive the addition of small quantum fluctuations? We will address this question within a spin wave calculation. Since the spin wave calculation is essentially identical for all $N \geq 2$, we specialize below to the O(2) model:

$$H = \frac{U}{2} \sum_i n_i^2 - J \sum_{\langle ij \rangle} \alpha_{ij} \cos(\phi_i - \phi_j). \quad (3)$$

The ϕ_i represent the phase of the bosons at site i . The operator n_i has integer eigenvalues and physically represents the excess boson number at each site. The ϕ_i and n_i on a site are conjugate variables:

$$[n_i, \exp i\phi_j] = \delta_{ij} \exp i\phi_i. \quad (4)$$

This model may also be taken to represent an array of Josephson junctions. U is a measure of the charging energy that induces quantum fluctuations of the phase, J is the strength of the Josephson coupling.

In the absence of quantum fluctuations ($U = 0$), the classical ground state is simply $\phi_i = \text{const.}$ The effect of turning on a small U/J may be addressed in a harmonic (“spin-wave”) approximation by simply expanding the cosine:

$$H_{sw} = \frac{U}{2} \sum_i n_i^2 + \frac{J}{2} \sum_{\langle ij \rangle} \alpha_{ij} (\phi_i - \phi_j)^2 \quad (5)$$

It is easier to work with the equivalent Euclidean (imaginary time) action:

$$\begin{aligned} S &= \int d\tau \sum_i \frac{1}{2U} (\partial_\tau \phi_i)^2 + \frac{J}{2} \sum_{\langle ij \rangle} \phi_i T_{ij} \phi_j \\ &= \frac{1}{2} \int d\bar{\omega} \left(\frac{\omega^2}{U} \delta_{ij} + J T_{ij} \right) \phi_i(\omega) \phi_j(-\omega) \end{aligned} \quad (6)$$

where we have rewritten the potential energy part using $T_{ij} = \alpha_{ij}(2\delta_{ij} - 1)$, and the frequency integral has $d\bar{\omega} = \frac{d\omega}{2\pi}$.

In this quadratic approximation, the superfluid order

parameter is readily calculated:

$$\begin{aligned} \langle \exp i\phi_i \rangle &= \exp\left(-\frac{1}{2} \langle \phi_i^2 \rangle\right) \\ \langle \phi_i^2 \rangle &= \int d\bar{\omega} \left[\left(\frac{\omega^2 \mathbf{1}}{U} + J\mathbf{T} \right)^{-1} \right]_{ii} \end{aligned} \quad (7)$$

$$= \sqrt{\frac{U}{J}} [\mathbf{T}^{-\frac{1}{2}}]_{ii} \quad (8)$$

Note that $\langle \phi_i^2 \rangle$ is formally of order $\sqrt{U/J}$. For small U/J , it will therefore be small so long as $[\mathbf{T}^{-\frac{1}{2}}]_{ii}$ is finite, and the long range order will survive quantum fluctuations. Below we will establish the required finiteness.

Eqn. 8 may be usefully rewritten in terms of the eigenvalues and eigenvectors of the matrix \mathbf{T} . Since \mathbf{T} is a real, symmetric positive semi-definite ($\mathbf{x}^T \mathbf{T} \mathbf{x} \geq 0$) matrix, it has real eigenvectors and eigenvalues (χ_n, λ_n) with $\lambda_n \geq 0$ (the zero eigenvalue is obtained for the uniform vector on connected sites):

$$\sum_j T_{ij} \chi_n(j) = \lambda_n \chi_n(i) \quad (9)$$

Clearly, this is just the eigenvalue problem for the Laplacian on the lattice defined by the α_{ij} , which in this case is taken to be at the percolation threshold. We get

$$\langle \phi_i^2 \rangle = \sum_n \frac{1}{\sqrt{\lambda_n}} [\chi_n(i)]^2 \quad (10)$$

The eigenvectors are assumed to be normalized on the percolation cluster:

$$\sum_{j \in \text{perc. cluster}} \chi_n^2(j) = 1 \quad (11)$$

To argue for the finiteness of the integral in Eqn. (10), we first consider the site averaged value of the RMS phase fluctuation:

$$\langle \phi^2 \rangle_{\text{Perc}} = \frac{1}{N_p} \sum_{i \in \text{Perc. cluster}} \langle \phi_i^2 \rangle \quad (12)$$

$$= \frac{1}{N_p} \sum_n \frac{1}{\sqrt{\lambda_n}} \quad (13)$$

Here N_p is the total number of sites on the incipient cluster and we have used Eq. (10), (11). In terms of the density of states per site $\rho(\lambda)$ for the eigenvalues of the operator \mathbf{T}

$$\rho(\lambda) = \frac{1}{N_p} \sum_n \delta(\lambda - \lambda_n) \quad (14)$$

we have:

$$\langle \phi^2 \rangle_{\text{Perc}} = \int_0^\infty d\lambda \frac{\rho(\lambda)}{\sqrt{\lambda}} \quad (15)$$

Finiteness (or lack thereof) of the phase fluctuations is determined by the behaviour of the density of states at very small λ . In the thermodynamic limit, the asymptotic behaviour of $\rho(\lambda)$ is known¹, since \mathbf{T} is proportional to the Laplacian on the percolation cluster. We have

$$\rho(\lambda) \sim \lambda^{\frac{d_s}{2}-1} \quad (16)$$

where d_s is called the *fracton* dimension. (On a regular one dimensional line, we note that $d_s = 1$, which gives the well known logarithmic divergence in the RMS value of the phase fluctuations). For percolation clusters in spatial dimension $d = 2$, $d_s = 1.32$ (see Ref.¹). In fact for percolation clusters in all dimensions, its value is very close to $4/3$.

Thus, for percolation in $d = 2$ we have:

$$\langle \phi^2 \rangle_{Perc} \sim \int d\lambda \lambda^{-0.84} \quad (17)$$

which is clearly finite when integrated over small λ . Since the fracton dimension of a percolation cluster does not vary much with spatial dimension, this finiteness of the site averaged RMS phase fluctuations holds for percolation in *any* dimension $d \geq 2$.

To reinforce this point, we turn to an alternate representation of the suppression of superfluid order in terms of the return probability of a random walker. Using a recent rigorous result for the latter, we can establish bounds on the former for an *any* site of the cluster, provided that we are away from threshold on the percolating side ($p < p_c$).

Consider a random walker placed on the percolation cluster, that begins its walk at site i . The differential equation describing the time evolution of the probability of this walker being found at time t at position j ($P_i(j, t)$) is:

$$\partial_t P_i(j, t) = -T_{jk} P_i(k, t) \quad (18)$$

where an appropriate choice of the stepping rate has been made. Thus, the probability of the particle returning to the site i where it started from is simply related to the eigenvalues and eigenfunctions of the Laplacian operator on the percolation cluster:

$$P_i(i, t) = \sum_n \chi_n^2(i) \exp(-\lambda_n t) \quad (19)$$

The root mean square (RMS) phase fluctuation amplitude at a site i (10) can be simply expressed in terms of this return probability $P_{ii}(t)$ as

$$\langle \phi_i^2 \rangle = \int_0^\infty dt \frac{P_i(i, t)}{\sqrt{\pi t}} \quad (20)$$

As a simple check of this formula, consider the case of a linear lattice, uniform, nearest-neighbor hopping $J_{ij} = J_{i,i+1} = J$. Then, the walker just performs a random walk in one dimension. If one takes the naive

continuum limit of (18), it is not hard to see that the return probability decays like $1/\sqrt{t}$ as $t \rightarrow \infty$. Applying (20), this implies the usual logarithmic divergence in the RMS phase fluctuations that destroys LRO in one dimensional superfluids¹⁷.

For some percolation clusters, Remy and Mathieu have found an upper bound for the asymptotic decay of the return probability.¹⁸ They considered site-percolation on the square lattice and looked at strictly $p < p_c$: the random walker has an infinite connected cluster to explore. They showed rigorously that for almost all cluster realizations, as $t \rightarrow \infty$,

$$P_i(i, t) < 1/t, \quad (21)$$

where, i refers to *any* site of the cluster. In other words, the asymptotic decay of the heat kernel on all sites of almost all cluster realizations, decays as fast as it does in the undiluted two-dimensional lattice. Using (20), this implies that for *any* site on the infinite cluster for $p < p_c$, the contribution to RMS phase fluctuations from asymptotically long time-scales is indeed finite, and bounded.

The two main results of this section suggest that long-range order has stability to weak quantum fluctuations. We established these results by making the spin-wave approximation to linearize the equations of motion. In the following section we introduce a complementary approach (the slow-blob approximation) that treats the non-linear dynamics beyond the spin-wave approximation.

III. SLOW BLOB APPROXIMATION TO O(N) MODEL AT $p = p_c$

Within the slow-blob approximation to the backbone, we proceed in two stages. In the first stage, we treat blob degrees of freedom as parameters rather than dynamical variables, and we solve the link problem for the ground-state energy $E(\{\vec{L}_i, \vec{n}_i\})$. Since links connect only to blobs (Fig. 1), the link problem reduces to that of independent links. In the second stage, we treat the ground-state energy $E(\{\vec{L}_i, \vec{n}_i\})$ as an adiabatic potential energy for the blobs, and solve for the blob ground-state.

An analogous procedure arises in the study of molecular vibration spectra, where it is called the Born-Oppenheimer approximation.¹⁹ In that case, the slow degrees of freedom, analogous to blobs, are the massive ion cores. The fast degrees of freedom, analogous to links, are outer shell electrons. Corrections to the Born-Oppenheimer approximation are suppressed by the ratio $m/M \approx 10^{-3}$, of electron to ion mass.

Here, the relevant control parameter is the ratio u/U of blob charging energy to bare charging energy. If the blobs are internally ordered then one has the simple relation

$$u = \frac{U}{n}, \quad (22)$$

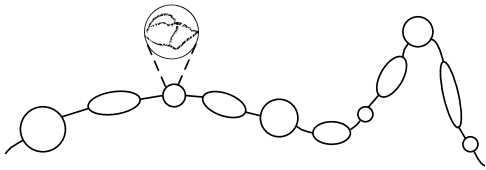


FIG. 1: The backbone of a percolation cluster is the union of self-avoiding walks on the cluster. It consists of blobs (ovals) connected by links. The internal structure of a blob (inset) shows that blobs consist of bonds which may be removed without disconnecting the cluster. In contrast, links consist of bonds which, if removed, disconnect the cluster.

where, n is the number of sites in a given blob. Now, on average, blobs are very big: $\langle n \rangle \approx L^{d_b-1/\nu}$, where L is the side-length of finite lattice.²⁰ See Table I, for estimates of ν and d_b . The bottom line is that, in two and three dimensions $d_b - 1/\nu > 0$. For $d_b > 1/\nu$, the blobs attached to the ends of a given link, have, on average, a thermodynamically small charging energy: $u \sim U/L^{d_b-1/\nu}$. Further, even the smallest blobs must contain at least four sites, so, even in the worst case the blob charging energy $u/U \approx .25$ is reasonably small.

This computation treats the blobs as internally ordered, which is a reliable approximation. If the blobs were not internally ordered, then the site-averaged RMS phase fluctuations $\langle \phi^2 \rangle_{\text{perc}}$ would not be finite. In section II, we showed in the spin-wave approximation that the fluctuations are finite (See (17)). Thus the blobs must be internally ordered, and our computation in the preceding paragraph can be trusted.

Following the idea of the slow-boson approximation, we consider the link problem with the blobs treated as parameters and determine $P(j)$ for $j \ll J$. Consider a given disorder realization of the α_{ij} in the bare Hamiltonian (1). Between two neighboring blobs, the link length ℓ will vary randomly. In fact, the lengths have an exponential distribution:^{20,21}

$$p(\ell) \sim \exp(-\ell/\ell_0), \quad (23)$$

with, for example, $\ell_0 \approx 2.7$ for square lattice percolation.²⁰ If we impose twisted boundary conditions with $\vec{n}_1 \neq \vec{n}_2$, the ground-state energy of the link increases by an ℓ -dependent amount:

$$E(\vec{n}_1, \vec{n}_2) \approx -j(\ell)\vec{n}_1 \cdot \vec{n}_2, \quad (24)$$

where, the “stiffness” $j(\ell)$, depends on the link length, ℓ and, implicitly, on the parameters of the bare model J, U in ((1)). From this we can deduce the distribution of blob exchange couplings $P(j)$ appearing in (2) by a simple change of variables:

$$P(j) = p(\ell) \left| \frac{dj(\ell)}{d\ell} \right|^{-1} \quad (25)$$

where, ℓ is the link length satisfying $j(\ell) = j$.

TABLE I: Correlation-length ν , backbone d_b , and blob-size α exponents for percolation in various dimensions d . For approximate results, number in parentheses indicates standard-deviation of last digit.

| d | 2 | 3 | ≥ 6 ^a |
|----------|--------------------------|------------------------|-----------------------|
| ν | $4/3$ ^b | $1.12(1)$ ^c | $1/2$ |
| d_b | $1.6431(6)$ ^c | $1.74(2)$ ^c | 2 |
| α | $0.5435(2)$ | $0.487(10)$ | 0 |

^aMean-field theory works for $d \geq 6$ and gives exact exponents, Ref. 23.

^bExact, see Ref. 24

^cRef. 20

^dRef. 25

It remains to compute the stiffness of a link. Fortunately, Cardy has computed $j(\ell)$.²² For $N = 2$, there are two qualitatively different cases to consider: large U ($U > \pi^2 J/4$) and small U ($U < \pi^2 J/4$). For large U , the link breaks into segments of length ξ with the property that rotors in different segments are essentially uncorrelated. In this “short-range” phase, the stiffness drops off exponentially with link length: $j(\ell) \sim \exp(-\ell/\xi)$. In contrast, for small U , the stiffness falls off only as ℓ^{-1} : $j(\ell) \rightarrow k/\ell$. For $N \geq 3$, there is only one case to consider, since for all values of U/J , the link is in a short-range phase with exponentially small stiffness.⁸ To summarize, the stiffness depends on link length as follows:

$$j(\ell) \sim \begin{cases} k/\ell, & N = 2, (\text{large } U) \\ e^{-\ell/\xi}, & N \geq 3, \text{ and } N = 2, (\text{small } U). \end{cases} \quad (26)$$

Plugging this into (25) gives the link strength distribution $P(j)$

$$P(j) \sim \begin{cases} e^{-k/\ell_0 j}, & N = 2, (\text{large } U) \\ j^{\xi/\ell_0-1}, & N \geq 3, \text{ and } N = 2, (\text{small } U). \end{cases} \quad (27)$$

The distribution $R(u)$ follows directly from the distribution of blob sizes n . For large n , the fraction of blobs with size n , scales like $n^{-2+\alpha}$, with $0 < \alpha < 1$, given in terms of backbone dimension, d_b and correlation length exponent ν via $\alpha = 1 - 1/(d_b \nu)$.²⁰ See Table I for estimates of α . Thus, we have determined the charging energy distribution entering (2), using (22) to change variables from blob size n to charging energy u :

$$R(u) \propto u^{-\alpha}, \quad (28)$$

where, $u \ll U$ is the charging energy of a given blob. We have now completely specified the blob problem (2).

The goal of this model (2) is to understand the competition between two possibilities: either very large blobs tend to “anchor” order across one-dimensional links, as has been suggested to explain ordering in the diluted 2D Heisenberg model, or else fluctuations within one-dimensional links destroy LRO. Both possibilities are realized in our model for different values of the initial dis-

tributions. For parameters chosen to reflect actual percolation clusters in 2D, our renormalization group calculation, described in section IV, finds LRO.

The next step is to see how this power-law distribution of blob sizes enhances ordering and leads to new fixed points in a real-space renormalization group calculation for disordered interacting bosons in 1D.

IV. RENORMALIZATION GROUP FLOW OF $O(2)$ MODEL FOR LARGE U

The idea of the real-space renormalization group for the $O(2)$ rotor in 1D is to successively integrate out either the largest Josephson coupling or the largest charging energy (See Appendix A for a description of the elementary renormalization group step and its generalization to the $O(N)$ case). This iterative procedure generates flow equations for the distributions of charging energy and Josephson coupling. The capacitance distribution is given as a function $f(\zeta)$ of the scaled variable $\zeta = \Omega/u - 1$, where Ω is an upper cutoff of energy: $\Omega = \max_i \{u_i, j_i\}$, and the Josephson coupling distribution is given as a function $g(\beta)$ of the scaled variable $\beta = \log(\Omega/j)$.

The analysis of one-dimensional models begins with the RSRG flow equations¹⁶ as a function of energy scale Γ for the charging energy distribution $f(\zeta, \Gamma)$ and Josephson coupling distribution $g(\beta, \Gamma)$:

$$\begin{aligned} \frac{\partial f}{\partial \Gamma} &= g_0 \int_0^\infty \int_0^\infty f(\zeta_1) f(\zeta_2) \delta(\zeta_1 + \zeta_2 + 1 - \zeta) d\zeta_1 d\zeta_2 \\ &+ (1 + \zeta) \frac{\partial f}{\partial \zeta} + (f_0 + 1 - g_0) f. \\ \frac{\partial g}{\partial \Gamma} &= f_0 \int_0^\infty \int_0^\infty d\beta_1 d\beta_2 g(\beta_1) g(\beta_2) \delta(\beta_1 + \beta_2 - \beta) \\ &+ \frac{\partial g}{\partial \beta} + g(g_0 - f_0). \end{aligned} \quad (29)$$

Here $\Gamma = \log(\Omega_I/\Omega)$ tracks the progress of the renormalization flow (Ω_I is the largest coupling in (2) before renormalization), $f_0 = f(0)$ and $g_0 = g(0)$. We will eventually discuss the behavior of the coupled f and g equations, but for now, consider g_0 as a constant parameter in the f flow equation.

It is possible to get immediate insight into the phase diagram found for exponential distributions¹⁶ by averaging both sides of the flow equation. The average $\langle \zeta \rangle = \int_0^\infty \zeta f(\zeta) d\zeta$, if it exists as for the exponential distributions considered in by Altamirano et. al.¹⁶, evolves as

$$\frac{d}{d\Gamma} \langle \zeta \rangle = g_0(1 + \langle \zeta \rangle) + f_0 \langle \zeta \rangle - 1 - \langle \zeta \rangle. \quad (30)$$

In this form, we can understand the appearance of a transition at $g_0 = 1$ for the class of distributions studied in [16]: for that one-parameter family of distributions $f_a(\zeta) = ae^{-\zeta/a}$, so that $f_0 = a$, we have $\langle \zeta \rangle = 1/a$ so

$$f_0 \langle \zeta \rangle - 1 - \langle \zeta \rangle = -1/a = -1/f_0. \quad (31)$$

The flow equation for the mean capacitance, if the function f is initially of the form f_a , is

$$\frac{d}{d\Gamma} \langle \zeta \rangle = g_0(1 + 1/a) - 1/a = g_0 + (g_0 - 1)/a. \quad (32)$$

The replacement $\delta(\zeta_1 + \zeta_2 + 1 - \zeta) \rightarrow \delta(\zeta_1 + \zeta_2 - \zeta)$ made in¹⁶ corresponds to replacing $g_0(1 + \langle \zeta \rangle)$ by $g_0 \langle \zeta \rangle$ in (30). With this replacement, an f distribution initially in the one-parameter family remains in this one-parameter family even for nonzero g_0 , and the average charging energy, a , flows as follows:¹⁶

$$\frac{da}{d\Gamma} = (1 - g_0)a. \quad (33)$$

This equation is written in terms of a rather than f_0 in order to stress that it is *specific to exponential distributions*. It is now shown that power-law distributions have a different RG equation with different qualitative behavior, leading to a significantly different phase diagram.

There are exact fixed points of the RG flow equation that are not contained in the family of exponential distributions that has been studied previously. Power-law distributions are needed both to describe these fixed points and to model the fractal distribution of blob sizes on the percolation cluster [See Eq. 28]. Setting $g_0 = 0$, we obtain a one-parameter family of static solutions of (29)

$$f_b(\zeta) = \frac{b}{(1 + \zeta)^{1+b}}. \quad (34)$$

These are well-behaved decreasing normalized distributions for all $b > 0$. For $b > 1$, the mean $\langle \zeta \rangle$ converges and satisfies

$$f_0 \langle \zeta \rangle - \langle \zeta \rangle - 1 = 0 \quad (35)$$

so that, as required, the mean is constant in time. Hence there is a one-parameter family of fixed points f_b that lies outside the one-parameter family f_a considered in [16], which contains no fixed points at finite a . Now if the function f is originally of the form f_b , the mean $\langle \zeta \rangle$ is increasing if $g_0 > 0$, suggesting that the system can flow to large capacitance (small charging energy) if $g_0 > 0$.

More explicitly, we simply evaluate the right-hand side of the flow equation (29) using our power-law distributions $f_b(\zeta)$, and find that the value of the distribution at large capacitance increases. That is, the distribution flows to large capacitance assuming that it starts out with a power-law form. For a power-law form, the integral appearing in (29) has the following simple, asymptotic behavior:

$$\int_0^\infty \int_0^\infty f_b(\zeta_1) f_b(\zeta_2) \delta(\zeta_1 + \zeta_2 + 1 - \zeta) d\zeta_1 d\zeta_2 \rightarrow 2f_b(\zeta), \quad (36)$$

for $\zeta \gg 1$. Using this fact, and the fact that at $g_0 = 0$, power-laws are fixed points of the flow, one finds that the $f_b(\zeta)$ distributions flow as follows at large capacitance:

$$\frac{\partial f_b}{\partial \Gamma} \rightarrow g_0 f_b(\zeta). \quad (37)$$

For $g_0 > 0$, the right-hand side is positive, and, as the result, the value of the distribution at large values of ζ increases under the flow. Thus, we see explicitly the tendency for power-law distributions to flow towards large capacitance (small charging energy).

So far we have seen that the mean $\langle \zeta \rangle$, assuming $g_0 = 0$, is constant for the family f_b and decreasing for the family f_a . There are also well-behaved distributions for which $f_0 \langle \zeta \rangle - \langle \zeta \rangle - 1 > 0$: an example is $f(\zeta) = 10(1 + \sqrt{\zeta})^{-6}$, for which $f_0 = 10$ and $\langle \zeta \rangle = 1$. However, one might wonder if the initial increase or decrease of the mean $\langle \zeta \rangle$ is a useful guide to the eventual behavior of the RG flow. To answer this question, Appendix B constructs additional soliton solutions, which include the fixed points $f_b(\zeta)$ as a limiting case, and for which the $g_0 = 0$ flow equation is exactly solvable. One family of solutions are related by a logarithmic rescaling of variables to solutions discussed by Fisher in the context of spin chains.¹⁵ The construction exhibits an interesting cumulant property of the nonlinear flow equation at $g_0 = 0$.

The previous paragraphs constructed a new set of fixed-point solutions, the $f_b(\zeta)$ in (34), to the functional RG equation with $g_0 = 0$. Appendix B gives other solutions to the $g_0 = 0$ equation for f , but no full solution to the coupled RG equations with f_0 and g_0 both nonzero has been found. Hence some other means of projecting the infinite-dimensional renormalization group flows to a finite-dimensional subspace is necessary. This section gives a prescription for this projection that both justifies the phase diagram found in [16] for exponential distributions and gives a new phase diagram once power-law tails in capacitance are allowed. The RG flows superficially depend on a cutoff introduced in the projection process, but the phase diagram and location of the critical point are cutoff-independent.

Let $0 < a < 1$ be some arbitrary cutoff, and define $0 \leq W_a \leq 1$ as the integral

$$W_a = \int_a^\infty f(\zeta) d\zeta. \quad (38)$$

The evolution equation for W_a is

$$\frac{dW_a}{d\Gamma} = f_0 W_a - (1+a)f(a) + g_0(1 - W_a). \quad (39)$$

Note that for $g_0 = 0$, the fixed-point solutions $f_b(\zeta)$ have $W_a = 1/(1+a)^b$ so that $dW_a/d\Gamma = 0$ correctly. In a moment we will consider the flow generated by this equation within the f_b , but first consider the exponential solutions $f(\zeta) = f_0 \exp(-f_0 \zeta)$. Substituting into (39) gives the projected flow

$$\frac{df_0}{d\Gamma} = f_0 - g_0 \frac{e^{af_0} - 1}{a}. \quad (40)$$

When f_0 is small, this equation becomes

$$\frac{df_0}{d\Gamma} = f_0 - f_0 g_0, \quad (41)$$

which is exactly the RG flow obtained in [16] under an approximation valid in this small- f_0 limit. The same equation is also obtained taking $a \rightarrow 0$ for any f_0 . For small f_0 , the superfluid transition in these equations at $g_0 = 1$ has been discussed thoroughly by Altman et al.¹⁶ The critical point $f_0 = 0, g_0 = 1$ corresponds to the transition between ‘‘stiff’’ and ‘‘floppy’’ regimes of the classical XY model.²⁶ This RG flow is shown in Fig. 1.

Now consider instead the flow within the power-law solutions f_b . For $g_0 \neq 0$, the evolution equation (39) defines a projected flow within the one-parameter subspace f_b : since $f_0 = f(0) = b$, we have

$$\frac{df_0}{d\Gamma} = -g_0 \frac{1 - W_a}{W_a \log(1+a)} = -g_0 \frac{\exp(f_0 \log(1+a)) - 1}{\log(1+a)}. \quad (42)$$

Again taking the limit of small f_0 and any a , or small a and any f_0 , we have

$$\frac{df_0}{d\Gamma} = -f_0 g_0. \quad (43)$$

Note that the right-hand-side is the same as in the previously obtained flow equation for *coupling strength*¹⁶

$$\frac{dg_0}{d\Gamma} = -f_0 g_0 \quad (44)$$

so that $f_0 - g_0$ is constant and the flows are as shown in Fig. 2. This coupling strength flow equation describes the flow within a power-law family of distribution of coupling strength $P(j) \propto j^{g_0-1}$. As argued in the previous section, such a distribution enters (2) for the $O(2)$ rotor model with large U [See Eq. 27)]. In the next section, we discuss the small U case.

Note that now there is no phase transition at the value $g_0 = 1$; instead there are two lines of fixed points, one with $f_0 = 0$ and one with $g_0 = 0$. The entire classical line $f_0 = 0$ is stable, including both the ‘‘stiff’’ and ‘‘floppy’’ regimes of the classical XY model. Now, we computed the initial conditions for this flow (See (27) and (28)):

$$\begin{aligned} f_0(\Gamma = 0) &= 1 - \alpha, \\ g_0(\Gamma = 0) &= \xi/\ell_0, \end{aligned} \quad (45)$$

where, ξ is the correlation length of a $O(2)$ rotor chain with large charging energy U , ℓ_0 is the average length of links of red sites, and, $\alpha = 1 - 1/(d_b \nu)$ is the blob exponent tabulated in Table I. Since $f_0 - g_0$ is a renormalization group invariant of the flow in (43,44), we can determine the fixed point towards which the flow tends in a simple way. Namely, the flow tends towards the ordered, classical line $f_0 = 0$ provided that initially we have $g_0(\Gamma = 0) > f_0(\Gamma = 0)$. That is, to have long-range order, we must tune U/J close enough to the Kosterlitz-Thouless transition of a *one-dimensional, clean* $O(2)$ rotor model at $U/J \approx \pi^2/4$, where ξ diverges, such that the following criterion is satisfied:

$$\xi > \ell_0(1 - \alpha) \quad (46)$$

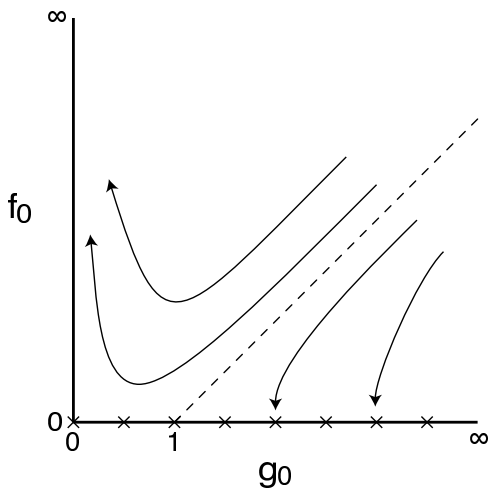


FIG. 2: Renormalization-group flows projected to two-parameter plane, after [16], for capacitance distributions with exponential damping at large capacitance.

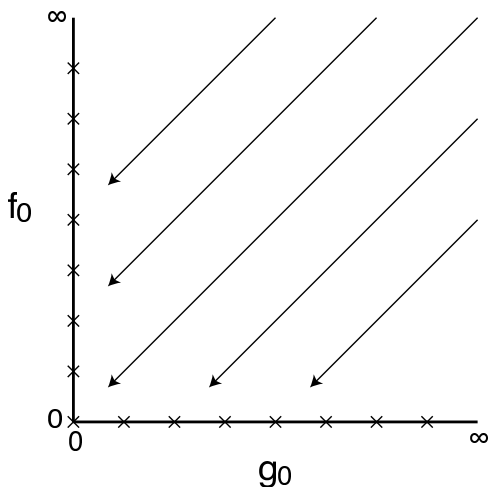


FIG. 3: Renormalization-group flows projected to two-parameter plane, for capacitance distributions with power-law damping at large capacitance. Note the new line of fixed points at $g_0 = 0$ and the absence of a phase transition at $(g_0, f_0) = (1, 0)$.

Further, when this criterion is not satisfied, the flow tends towards the insulating line of fixed points $g_0 = 0$. Thus, the blob hamiltonian (2) admits both insulating and superfluid ground-states. When U/J is small enough to satisfy criterion (46), the renormalization group flow tends to the superfluid ground-state. The possibility of an ordered phase stable to nonzero charging energy is novel, and supports the existence of order for the $O(2)$ rotor model on percolation clusters via the connection discussed in the Introduction.

V. $O(2)$ ROTOR FOR SMALL U

In this section, we consider the special case of the $O(2)$ rotor with small U , at percolation threshold, that is, (1) with $N = 2$. We will argue that this case is only slightly different than the large U case considered in the previous section. Namely, we will show using a spin-wave argument and a real-space renormalization group argument, that this case exhibits long-range order regardless of the value U/J , so long as U is small. Recall that, by contrast, for large U , one must satisfy the criterion (46) for the ground-state to exhibit long-range order.

As in the previous section, we begin with the slow-blob approximation (2). In this approximation, the novelty of the $O(2)$ rotor with small U arises from the “activated” form of the exchange distribution $P(j)$ in (27):

$$P(j) \sim e^{-k/\ell_0 j}, \quad (47)$$

In other words, the power-law charging energy distribution (28) holds for this case too. Only the exchange distribution changes compared to the large U case. Notice that the new, activated exchange distribution is significantly less broad than the power-law distributions considered in the previous section.

Let us, to first approximation, neglect completely the spread in the exchange distribution, for this activated form. This is a drastic approximation which we will improve upon below by considering the flow of the distribution under real-space renormalization. However, the activated form (47) is quite narrow, and treating it as completely concentrated at its mean-value will turn out to be a consistent approximation. In this approximation, we may use the following exact result for the asymptotic decay of the (appropriately defined) return probability of a random walker:

$$\langle P_i(i, t) \rangle \rightarrow \left(\frac{1}{\sqrt{t}}\right)^{\frac{1}{1-\alpha/2}}. \quad (48)$$

Alexander et. al.²⁷ show that this result obtains for uniform exchange distribution and power-law charging energy distribution $R(u) \propto u^{-\alpha}$, with $0 < \alpha < 1$. Recall, that this range of α obtains for percolation in two and three dimensions (See table I). Using (20), which applies to (2), the asymptotic result in (48) implies a finite RMS phase fluctuation of the blob phases ϕ_i , where, the blob’s rotor variable in (2) is given by $\vec{n}_i = (\cos(\phi_i), \sin(\phi_i))$, for $N = 2$ rotor. Thus, in the approximation of uniform exchange energy, spin-wave theory predicts that (2) exhibits an ordered phase stabilized by the small- U part of the charging energy distribution.

Let us now consider the actual distribution (47) and see how it flows under real-space renormalization. As in the previous section, we gain immediate insight into the flow by averaging both sides of the flow equation (29). The average $\langle \beta \rangle = \int_0^\infty \beta g(\beta) d\beta$ exists for activated distributions (47) and evolves as follows:

$$\frac{d}{d\ell} \langle \beta \rangle = -1 + (g_0 + f_0) \langle \beta \rangle. \quad (49)$$

Recall, that $\beta = \log(\Omega/j)$ is the scaled Josephson exchange and $g(\beta) = P(j = \Omega e^{-\beta})\Omega e^{-\beta}$ is the distribution of β , where, $P(j)$ is given by (47). More directly, the activated ansatz (47) implies a distribution of β of the following form:

$$g(\beta, \Gamma) = g_0(\Gamma)e^{-g_0(\Gamma)e^{\beta} - \beta + g_0(\Gamma)}, \quad (50)$$

Here, $\Gamma = \log(\Omega_I/\Omega)$ is the flow parameter, where, $\Omega_I = \max\{j_i, u_i\}$ is the largest coupling in (2) before any renormalization, and $\Omega \leq \Omega_I$ is the largest coupling at the current stage of renormalization. The parameter, $g_0(\Gamma)$ *initially* satisfies $g_0(\Gamma = 0) = k/\ell_0\Omega_I$. At later times, we can evaluate how $g_0(\Gamma)$ flows by first computing the expectation appearing in (49):

$$\langle \beta \rangle = e^{g_0(\Gamma)} E_1(g_0(\Gamma)). \quad (51)$$

Here, the exponential integral appears: $E_1(g_0) = \int_{g_0}^{\infty} d\gamma e^{-\gamma}/\gamma$. Substituting (51) into (49) gives the projected flow of $g_0(\Gamma)$:

$$\frac{dg_0}{d\Gamma} = \frac{-1 + (f_0 + g_0)e^{g_0} E_1(g_0)}{-1 + g_0 e^{g_0} E_1(g_0)} g_0. \quad (52)$$

When g_0 is small, the flow simplifies to the following:

$$\frac{dg_0}{d\Gamma} = g_0 + f_0 g_0 \ln g_0 + \dots, \quad (53)$$

where, the omitted terms are higher order in g_0 . The right-hand side of (53) is initially positive, so g_0 grows under renormalization. Recall, that g_0 is the weight of the distribution at the *large* values of the exchange strength j . The projected flow equation (53) implies that our activated form (47) flows towards a narrower distribution concentrated at the largest values of j . This justifies the spin-wave treatment at the beginning of this section (Eq. (48) and paragraph containing it), which assumed a narrow distribution of j .

Thus, the conclusion suggested by spin-wave theory holds even when we allow the exchange distribution to start with an activated form. Since this is precisely the form of distribution satisfied by the $O(2)$ rotor with $U/J < \pi^2/4$, the model must have finite RMS fluctuations of the blob rotor variables \vec{n}_i . In the slow-blob approximation, this implies that the percolation cluster as a whole exhibits long-range order for the $O(2)$ rotor model with $U/J < \pi^2/4$.

VI. CONCLUSION

To conclude, the question of whether the $O(N)$ ($N \geq 2$) quantum rotor model can have an ordered phase on the percolation cluster was studied via a spin wave calculation and via a real-space renormalization group calculation. The result for these models may be summarized in the following way which also tracks the details of the

calculation. We associate with the incipient percolation cluster an effective spatial dimensionality in order to discuss the question of ordering. The correct spatial dimensionality for this purpose is the *fracton* dimension d_s , defined in equation (16) from the spectral density of the Laplacian on the percolation cluster. This dimensionality d_s is distinct from the fractal dimension of the percolation cluster, and happens to be numerically very close to $4/3$ for percolation in any dimension. The possibility of long range order can now be determined by simply comparing this dimension with the lower critical dimension arising from the Hohenberg-Mermin-Wagner theorem.¹⁷ Thus, for the zero temperature quantum models where $d_s + 1 > 2$ we have the possibility of long range order for percolation in any dimension, while at finite temperatures, these models are always disordered since $d_s < 2$.

The presence of weak links compelled us to investigate further the possibility of long range order. We “integrated” out the weak links, generating a low-energy description [See Eq. (2)], amenable to real-space renormalization. The renormalization group flow [See Fig. 3 and Eq. (43),(44)] demonstrated a competition between two natural length-scales associated with the links [See Eq. (46)]. On the one hand, the average length of a link ℓ_0 , and on the other, the correlation length within a long link ξ . The final result may be stated simply: When U/J is small enough that $\xi > \ell_0(1 - \alpha)$, then correlations “jump” across the weak links and create long-range order. The renormalization-group flow supporting this conclusion depends crucially on the fractal structure of the percolation backbone.

These considerations are summarized in the phase diagrams in Fig. 4. In Fig. 4(a), the existence of a finite superfluid order parameter at the percolation transition for small U/J leads to the vertical phase boundary. In Fig. 4(b), we simply point out that the well-known absence of a Mott insulating state for incommensurate filling at zero dilution persists under dilution until percolation threshold. Finally, the absence of superfluid order at finite temperatures on percolation clusters in any dimension $D \geq 2$ gives rise to the phase diagram shown in Fig. 4(c).

Acknowledgments

This project was inspired by scintillating discussions with Antonio Castro Neto, G. Refael, O. Motrunich, E. Altman, E. Mucciolo and C. Chamon, for which we are grateful. We thank E. Mucciolo and C. Chamon for also sharing their results prior to publication. This work was supported by NSF DMR-0238760 and the Hellman Foundation (N. B.-A. and J. E. M.), a Pappalardo Fellowship (AV) and by the MRSEC program of the NSF under DMR-0213282 (TS). TS also acknowledges support from the Alfred P. Sloan Foundation, The Research Corporation, and NEC corporation.

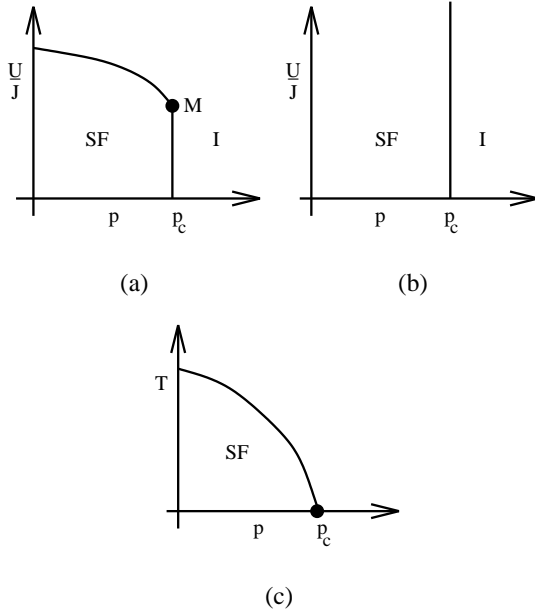


FIG. 4: The phase diagram for bosons with onsite repulsion on a diluted lattice as a function of the dilution fraction p . The percolation transition occurs at p_c . (a) Integer filling at zero temperature: The Mott insulating phase arises when charging energy U is large compared to Josephson coupling J . (b) Away from integer filling, the Mott phase is not present for any U/J . (c) Finite temperature transition for bosons out of the superfluid phase.

APPENDIX A: RG OF RANDOM $O(N)$ CHAIN

Consider the $O(N)$ rotor chain with random exchange and “charging” given in Eq. (2). We have two possible rg steps. First, if the largest energy is an exchange J_i , then we lock the two rotors together, and estimate the effective charging energy of the combined rotor. The result is that inverse charging energies add:

$$\tilde{U}^{-1} \approx U_i^{-1} + U_{i+1}^{-1} \quad (\text{A1})$$

Second, the largest energy may be a charging energy $\Omega = U_i$. In this case, we put this rotor in the rotationally invariant ground-state, and treat the neighboring rotors as a classical magnetic field $\vec{h} = J_i \vec{n}_i + J_{i+1} \vec{n}_{i+2}$. For small $|\vec{h}|/\Omega$, the ground-state energy is, to lowest order, $2h^2/N(N-1)\Omega$. Expanding this, yields a new effective coupling between the neighboring rotors:

$$\tilde{j} \approx \frac{4J_i J_{i+1}}{N(N-1)\Omega} \quad (\text{A2})$$

The first step is identical to $O(2)$ case. The second step is virtually identical. If we measure exchanges on a logarithmic scale, $\beta_i = \log(\Omega/J_i)$, then the $\Omega = U$ step becomes

$$\tilde{\beta} = \beta_i + \beta_{i+1} + \log(N(N-1)/4). \quad (\text{A3})$$

As always, in asymptotic analysis of these kind of flow equations, we can neglect additive constants in the RG-step, since we are looking for broadly distributed fixed points.¹⁵ In conclusion, we have obtained the elementary RG-step for the $O(N)$ rotor chain with strong disorder.

APPENDIX B: ADDITIONAL SOLUTIONS OF THE RSRG FLOW EQUATION

The goal of this section is to find Γ -dependent exact solutions of the capacitance flow equation (29) that verify the statements in Section III derived using projected RG flows. Although we have not been able to solve the nonlinear PDEs for arbitrary initial data, the exact solutions now discussed are examples supporting the qualitative behavior found using a moment equation in Section III. Let us look for a solution in terms of a distribution $\phi(b, \Gamma)$ over the one-parameter family $f_b(\zeta)$:

$$f(\zeta, \Gamma) = \int_0^\infty \phi(b, \Gamma) f_b(\zeta) db = \int_0^\infty \phi(b, \Gamma) \frac{b}{(1+\zeta)^{1+b}} db. \quad (\text{B1})$$

Now $f_0(\Gamma) = f(0, \Gamma) = \int_0^\infty b \phi(b, \Gamma) db$, i.e., the average $\langle b \rangle_\phi$ taken over the distribution $\phi(b, \Gamma)$. Our goal will be to find solutions of the evolution equation for $\phi(b, \Gamma)$:

$$\frac{\partial \phi(b, \Gamma)}{\partial \Gamma} = \left(-b + \int_0^\infty \phi(b_2) b_2 db_2 \right) \phi(b, \Gamma). \quad (\text{B2})$$

Now assume that $\phi(b, \Gamma)$ is nonnegative (it is then automatically normalized to 1) so that it can be regarded as a probability distribution. Its normalization is constant, and its mean (equal to f_0) evolves via

$$\frac{d\langle b \rangle_\phi}{d\Gamma} = \langle b \rangle_\phi^2 - \langle b^2 \rangle_\phi. \quad (\text{B3})$$

In terms of the mean μ_1 and the variance μ_2 , this equation is compactly written $\frac{d\mu_1}{d\Gamma} = -\mu_2$. A bit of algebra confirms that a similar evolution holds for all cumulants:

$$\frac{d\mu_n}{d\Gamma} = -\mu_{n+1}. \quad (\text{B4})$$

This provides a way to find soliton-like solutions. One class of solutions starts from the generalized Poisson distribution with two parameters λ and x_0 ,

$$\phi(b) = \sum_{k=0}^{\infty} \delta(b - kx_0) \frac{\lambda^k e^{-\lambda}}{k!} \quad (\text{B5})$$

which has cumulants $\mu_n = \lambda x_0^n$. This distribution has a finite probability of $b = 0$, which corresponds to exactly 0 charging energy; below we find a different soliton solution without this property. The discrete distribution (B5) approaches a continuous Gaussian centered at $b = b_0$ if we take the limits $x_0 \rightarrow 0$ and $\lambda \rightarrow \infty$ with $\lambda x_0 = b_0$. Then

the cumulant evolution equations are all solved if x_0 is constant and $\lambda(\Gamma)$ solves

$$\frac{d\lambda}{\Gamma} = -x_0\lambda \Rightarrow \lambda(\Gamma) = \lambda(0)e^{-x_0\Gamma}. \quad (\text{B6})$$

In the limit of small x_0 with $x_0\lambda(0)$ fixed, we recover the fixed-point solutions found previously.

A second family of solutions starts from the gamma distribution with parameters α and θ :

$$\phi(b) = \frac{b^{\alpha-1}e^{-b/\theta}}{\Gamma(\alpha)\theta^\alpha}. \quad (\text{B7})$$

The cumulants of the above distribution are

$$\kappa_n = \Gamma(n)\alpha\theta^n. \quad (\text{B8})$$

So, if the only Γ dependence is in θ ,

$$\frac{d\kappa_n}{d\Gamma} = \Gamma(n+1)\alpha\theta^{n-1}\frac{d\theta}{d\Gamma} = -\alpha\theta^{n+1}\Gamma(n+1) = -\kappa_{n+1} \quad (\text{B9})$$

if

$$\frac{d\theta}{d\Gamma} = -\theta^2 \Rightarrow \theta(\Gamma) = \frac{1}{\Gamma + \theta(0)^{-1}}. \quad (\text{B10})$$

It is simple to confirm explicitly that the resulting form for f ,

$$f(\zeta, \Gamma) = \frac{\alpha\theta(\Gamma)}{(1+\zeta)(1+\theta(\Gamma)\log(1+\zeta))^{\alpha+1}}, \quad (\text{B11})$$

is normalized for $\alpha > 0$ and satisfies the evolution equation. For this solution, $f_0(\Gamma) = \alpha/(\Gamma + \theta(0)^{-1})$, indicating that this charging energy distribution is marginally irrelevant even as $g_0 \rightarrow 0$, well away from the classical transition.

We also note that the gamma solutions have normalized variance $\kappa_2/(\kappa_1)^2 = 1/\alpha$, which is a constant of the motion. As $\alpha \rightarrow 0$, the distributions become extremely broad, and the RG is expected to be valid in this limit.

These two families of solutions suggest that having a finite probability of zero charging energy, as in the Poisson case, leads to an exponentially rapid flow of the entire distribution to zero charging energy: the order is strongly “nucleated” by the classical rotors with zero charging energy. The gamma solutions also flow to zero charging energy, proving that such flow is possible for regular distributions, but this solution flows only as a power-law. Note that the flow equation for θ is exactly that for a marginally irrelevant operator.

-
- ¹ D. Stauffer and A. Aharony, *Introduction to Percolation Theory* (Taylor and Francis, New York, 1992).
- ² S. Smirnov and W. Werner, *Math. Research Letters* **9**, 729 (2001).
- ³ O. P. Vajk, P. K. Mang, M. Greven, P. M. Gehring, and J. W. Lynn, *Science* **295**, 1691 (2002).
- ⁴ B. Mandelbrot, *The Fractal Geometry of Nature* (W. H. Freeman, 1982).
- ⁵ K. M. Lang, V. Madhavan, J. E. Hoffman, E. W. Hudson, H. Eisaki, S. Uchida, and J. C. Davis, *Nature* **415**, 412 (2002).
- ⁶ A. W. Sandvik, *Phys. Rev. B* **66**, 024418 (2002).
- ⁷ R. Yu, T. Roscilde, and S. Haas, *cond-mat/0410041*.
- ⁸ S. Sachdev, *Quantum phase transitions* (Cambridge, 2000), pp. 20–26 and 295–296.
- ⁹ A. W. Sandvik and M. Vekic, *Phys. Rev. Lett.* **74**, 1226 (1995).
- ¹⁰ Y. Chen and A. H. C. Neto, *Phys. Rev. B* **61**, R3772 (2000).
- ¹¹ E. Mucciolo, A. C. Neto, and C. Chamon, *Phys. Rev. B* **69**, 214424 (2004).
- ¹² A. Coniglio, *Phys. Rev. Lett.* **46**, 250 (1981).
- ¹³ R. Birgeneau, R. Cowley, G. Shirane, and H. Guggenheim, *Phys. Rev. Lett.* **37**, 940 (1976).
- ¹⁴ T. Senthil and S. Sachdev, *Phys. Rev. Lett.* **77**, 5292 (1996).
- ¹⁵ D. Fisher, *Phys. Rev. B* **50**, 3799 (1994).
- ¹⁶ E. Altman, Y. Kafri, A. Polkovnikov, and G. Refael, *Phys. Rev. Lett.* **93**, 150402 (2004).
- ¹⁷ P. C. Hohenberg, *Phys. Rev.* **158**, 383 (1967).
- ¹⁸ P. Mathieu and E. Remy, *math.pr/0301213*.
- ¹⁹ J. Ziman, *Principles of the Theory of Solids* (Cambridge, 1971), pp. 200–203.
- ²⁰ H. J. Herrmann and H. E. Stanley, *Phys. Rev. Lett.* **53**, 1121 (1984).
- ²¹ A. Coniglio, *J. Phys. A* **15**, 3829 (1982).
- ²² J. L. Cardy, *Scaling and renormalization in statistical physics* (Cambridge, 1996), pp. 125–126.
- ²³ S. Havlin and A. Bunde, in *Fractals and disordered systems*, edited by A. Bunde and S. Havlin (Springer-Verlag, 1991.).
- ²⁴ M. P. M. den Nijs, *J. Phys. A* **12**, 1857 (1979).
- ²⁵ J. L. Jacobsen and P. Zinn-Justin, *J. Phys. A* **35**, 2131 (2002).
- ²⁶ J. Straley, *J. Phys. C* **15**, 2343 (1982).
- ²⁷ S. Alexander, J. Bernasconi, W. Schneider, and R. Orbach, *Rev. Mod. Phys.* **53**, 175 (1981).